Particuology 22 (2015) 39–51

Contents lists available at ScienceDirect

Particuology

journal homepage: www.elsevier.com/locate/partic

Estimation of particle dynamics in 2-D fluidized beds using particle tracking velocimetry

Thomas Hagemeier[a,*], Christoph Roloff[b], Andreas Bück[a], Evangelos Tsotsas[a]

[a] NaWiTec, Thermal Process Engineering, Otto-von-Guericke University Magdeburg, Universitaetsplatz 2, 39106 Magdeburg, Germany
[b] Fluid Dynamics and Technical Flow, Otto-von-Guericke University Magdeburg, Universitaetsplatz 2, 39106 Magdeburg, Germany

ARTICLE INFO

Article history:
Received 6 May 2014
Received in revised form 31 July 2014
Accepted 16 August 2014

Keywords:
Particle dynamics
Particle tracking velocimetry
Pseudo-2D
Fluidized bed

ABSTRACT

The experimental characterization of particle dynamics in fluidized beds is of great importance in fostering an understanding of solid phase motion and its effect on particle properties in granulation processes. Commonly used techniques such as particle image velocimetry rely on the cross-correlation of illumination intensity and averaging procedures. It is not possible to obtain single particle velocities with such techniques. Moreover, the estimated velocities may not accurately represent the local particle velocities in regions with high velocity gradients. Consequently, there is a need for devices and methods that are capable of acquiring individual particle velocities. This paper describes how particle tracking velocimetry can be adapted to dense particulate flows. The approach presented in this paper couples high-speed imaging with an innovative segmentation algorithm for particle detection, and employs the Voronoi method to solve the assignment problem usually encountered in densely seeded flows. Lagrangian particle tracks are obtained as primary information, and these serve as the basis for calculating sophisticated quantities such as the solid-phase flow field, granular temperature, and solid volume fraction. We show that the consistency of individual trajectories is sufficient to recognize collision events.

Introduction

In granular systems, knowledge of the individual particle and particle cluster velocities is essential for a model-based description of particulate processes. For instance, the classical two-compartment modeling approach of granulation processes used by Börner, Peglow, and Tsotsas (2013) relies on particle velocities. These are used to determine residence times within two characteristic zones, and the solid mass fluxes between them, under spraying and drying processes. This topic was addressed numerically by Fries, Antonyuk, Heinrich, and Palzer (2011), and a recent experimental treatment was reported by Börner, Hagemeier, Ganzer, Peglow, and Tsotsas (2014). Therefore, an accurate quantification of particle velocities within the process chamber is of enormous value to modern macroscopic modeling approaches.

There are numerous methods of gathering information concerning particle velocities in fluidized beds (Bhusarapu, Al-Dahhan, & Duduković, 2006). Various measurement devices can be used, such as fiber optical probe, laser-Doppler velocimetry, or particle image velocimetry, as summarized by Werther (1999). Each technique has advantages and limitations. In this paper, we apply particle tracking velocimetry (PTV) to dense particulate flows in a pseudo-2D fluidized bed. To date, the PTV technique has been used to measure particle velocities in vibrating beds, Couette flows in shear cells, rotating drums, or during hopper discharge. These contributions considerably improved the application of PTV in the field of granular flows. However, to the best of our knowledge, PTV has not previously been applied to the complex flows found in fluidized beds, where densely packed particle clusters exist alongside loose particles in large gas bubbles. An additional layer of complexity arises from particle trajectories in opposing directions, as well as through inter-particle and particle-wall collisions. These aspects have not been captured by other measurement devices for larger particle systems. Therefore, the objectives of this communication are to: (i) report the use of PTV for dense gas–solid two-phase flows in bubbling fluidized beds, and (ii) describe the particle trajectories measured by this method.

This proof-of-concept study is structured as follows. "Particle tracking velocimetry" section gives a general introduction to the methodology of particle tracking velocimetry, and discusses two

* Corresponding author. Tel.: +49 391 6712322.
E-mail address: Thomas.Hagemeier@ovgu.de (T. Hagemeier).

http://dx.doi.org/10.1016/j.partic.2014.08.004

Nomenclature

d_p	particle diameter, m
f_r	frame rate, Hz
s_f	scale factor, pixel/mm
t, Δt	time, time step size, s
x, y, z	coordinates, pixel or m
I_A	interrogation area, m^2
$I_{1,2}$	images 1 and 2
$S_{i,j}$	Voronoi star i, j
T_{gran}	granular temperature, m^2/s^2
u_{mf}	minimum fluidization velocity, m/s

Greek symbols

ε_p	solid volume fraction,–
μ	fluid viscosity, kg/(m s)
ρ_p	particle density, kg/m^3
σ	standard deviation of particle velocity, m/s
τ	trajectory lifetime, s
τ_{corr}	corrected trajectory lifetime, s
τ_c	collision time, s
τ_v	particle response time, s

Abbreviations

FOV	field of view
PIV	particle image velocimetry
PTV	particle tracking velocimetry

approaches applicable to dense two-phase flows. In "Proposed PTV algorithm" section, we describe the PTV algorithm used in our investigations, including information on particle segmentation, tracking, and post-processing. "Experimental setup" section gives the experimental setup, with all operating conditions and hardware parameters, and "Results and discussion" section presents the resulting particle trajectories and derived quantities. More detailed results in the form of time series are given in Appendix A and as supplementary material (video sequences) online. In "Conclusions" section, we draw together some significant conclusions, and mention several open questions and ideas for future work.

Particle tracking velocimetry

PTV is an image-based measurement technique to quantify flow velocities. It is mainly applied in the field of fluid mechanics, in particular to liquid flows (Adrian, 1991; Lloyd, Ball, & Standsby, 1995). However, some researchers have also described PTV measurements in particulate multiphase flows. Capart, Young, and Zech (2002) identified three aspects of granular flows that restrict an out-of-the-box application of PTV. These challenges arise because granular flows are: (i) highly dense particulate systems, with (ii) fluctuating particle motions due to particle-particle collisions, resulting in discontinuous path lines, and (iii) sharp velocity gradients. Consequently, the methodology of PTV cannot be applied to dense particulate flows, such as in fluidized beds, without suitable modifications. First, the particle system has to be accessible for the high-speed camera and the illumination source. These two devices observe and illuminate the scene through a transparent wall. The opaqueness of the particle system restricts the application of PTV to pseudo-2D configurations. Moreover, the high particle density leads to correspondence problems within the tracking algorithm. To avoid erroneous results, particles need to be identifiable. This can be achieved in two ways. The moving particle bed could be seeded with particles that have a different optical property to the majority of particles. This would involve tracer particles being colored using paint or a fluorescent dye (e.g., Natarajan, Hunt, & Taylor, 1995), which is also a common way to improve the PTV technique for gas flows (Bendicks et al., 2011). A standard tracking algorithm could then be applied, because the concentration of tracer particles is low enough to identify the same tracer particle on subsequent images. The second technique uses a specialized imaging method in which the particles are segmented and a certain type of bed structure can be identified. In particular, the Voronoi imaging method is used to generate a net of connection lines between neighboring particles, yielding a specific pattern in the particle bed. Particle assignment and tracking is linked to the properties of the Voronoi diagram. Jesuthasan, Baliga, and Savage (2006) provided a comprehensive review of PTV techniques together with the principles of PIV applied to granular flows. They also indicated the use of pattern matching algorithms to solve the correspondence problem in granular or densely seeded flows.

PTV with colored tracers

Colored tracers are commonly applied in PTV to enable particle identification in dense particulate flows. The dilute and dense regions of discrete multiphase flows, such as the gas–solid two-phase flows typically found in pneumatic conveying or fluidized beds, can be distinguished on the basis of a time scale analysis. If the collision time τ_c is larger than the particle response time τ_v, particles have enough time to adapt to the flow velocity before they come into contact with another particle. Hence, the two-phase flow can be described as a dilute system when $\tau_v/\tau_c < 1$. When $\tau_v/\tau_c > 1$, the collision time is smaller than the particle response time. This is characteristic of a flow that is dominated by particle interactions, and is consequently described as a dense multiphase flow.

Both the response time and collision time are functions of material properties such as the solid and fluid densities, fluid viscosity, and particle size. However, an explicit expression for the response time τ_v is only available for the Stokes flow regime (low particle Reynolds number).

$$\tau_v = \frac{\rho_p d_p}{18\mu} \tag{1}$$

In contrast, the collision time is the inverse of the collision frequency $\tau_c = 1/f_c$, where f_c is a function of the particle diameter, relative velocity, and particle number density of one size class. This quantity is commonly estimated on the basis of collision models, as by Sommerfeld (2001). More details on phase properties and phase interactions are given in various textbooks (e.g., Crowe, 2006; Crowe, Sommerfeld, & Tsuji, 1998). Hsiau and Jang (1998) measured particle velocity fluctuations in a Couette flow using 2% colored tracer particles among a majority of equally sized non-colored particles. They observed the particle motion while shearing the powder, and found anisotropic velocity fluctuation distributions. This contradicts the general assumption of the kinetic theory of granular flow, according to which fluctuations are random and isotropic (Lun, Savage, Jeffrey, & Chepurniy, 1984). Moreover, the overall particle motion should be almost deterministic, with no spontaneous changes of direction observed. Natarajan et al. (1995) used colored tracer particles to observe granular flow behavior in a hopper. They also used 2% (by weight) black tracer particles to seed the flow.

Colored tracer particles were used by Chung, Hsiau, Liao, and Ooi (2010) to estimate the translational and rotational velocities of non-spherical particles (two bonded spheres of identical size) in a vibrating bed. They used a cross-correlation algorithm that accounts for particle rotation and translation by shifting and rotating a control window in two consecutive images. The method was

shown to be quite efficient, and yielded a broad range of quantitative data, including fluctuation velocities, granular temperatures, diffusion coefficients, and convection flow rates. In the literature, the amount of colored tracer particles is always below 8% of the total particle mass. This value was experimentally identified as the upper limit for the tracer concentration by Hsiau and Jang (1998).

PTV based on the Voronoi method

Particle tracking based on the Voronoi imaging method assumes that patterns formed by the particles within the fluidized bed exist over a certain period of time. A Voronoi diagram is a fragmentation of an area (in this case, the image taken by the high-speed camera) into a number of polygons (Aurenhammer, 1991). Each polygonal area is located around a centroid, with the restriction that each point within a polygon should be closer to its own centroid than to any other centroid. The connection of one centroid with all neighboring centroids is called a Voronoi star, and plays a key role in the evaluation procedure. A comprehensive description of the Voronoi method for granular flows is given by Capart et al. (2002), and will be summarized "Proposed PTV algorithm" in section.

The method can be applied to 2D and 3D flows, although near-wall regions may present difficulties in the case of dense particle packing. Stereoscopic images can be obtained using one camera to capture two perspectives in one image through a complex mirror arrangement, or by two synchronized cameras (Spinewine, Capart, Larcher, & Zech, 2003). The 3D approach enables the investigation of all three velocity components, as well as an estimation of the volumetric solid concentration. This requires special treatment to resolve the particle positions and overcome occlusion effects.

Luchnikov, Medvedev, Oger, and Troadec (1999) suggested a generalization of the Voronoi–Delaunay analysis to include non-spherical particles. Despite the fact that they did not couple their approach to a particle tracking algorithm, the authors proved the applicability of Voronoi-based PTV techniques to non-spherical particle shapes.

Another application was proposed by Chou and Lee (2009), who analyzed the flow behavior of dry particles in rotating drums. The resulting flow regimes were captured via high-speed imaging. The images were then processed by means of a PTV-Voronoi algorithm adopted from the work of Capart et al. (2002). As a result, Chou and Lee (2009) proposed a unique dimensionless flow parameter that accounts for the combined effects of gravity, particle velocity, particle size, and filling level.

Aleixo, Soares-Frazão, and Zech (2011) applied the PTV-Voronoi technique to a system of coated seeding particles to investigate velocity profiles in a dam-break situation. This contribution does not describe a granular flow, but provides an example of the potential for this methodology to be used for various applications.

To capture the whole region of interest while simultaneously resolving the particles, Spinewine and Zech (2001) used two synchronized cameras. They reported results for granular hopper flow based on the PTV-Voronoi method, and emphasized the importance of precise image stitching for accurate flow-field representation, showing that meaningful information can be obtained by dividing the region of interest into smaller sub-domains for individual evaluation. This method allowed the particle track properties to be described statistically and the derivation of averaged results.

These contributions show the potential of PTV combined with Voronoi mapping in the field of granular flows. However, hardware limitations mean that no application has yet considered the complex, transient, and dense flow in fluidized beds. In the following, an extended PTV algorithm for this situation is described in detail.

Proposed PTV algorithm

The PTV algorithm used in our study consists of several sequential steps, including particle segmentation, particle assignment using Voronoi cell matching, filter operations, and further post-processing. All raw images are corrected in advance for homogeneous intensity by subtracting a background image.

Particle segmentation

In contrast to other segmentation approaches, we do not use a gray level threshold or gradient to identify individual particles. Particles are identified by correlating a sample particle image with every raw image of the actual series. The sample particle image is a manually chosen section of the first image in a corresponding image sequence, as shown in Fig. 1. It is bounded so that the sample particle is captured completely in the image, but most of the background is excluded. The particle image is 28×28 pixel, and the raw image is 1024×1024 pixel. The sample particle image size ensures the complete enclosure of the sample particle owing to geometrical calibration with a calibration factor of $s_f = 14.43$ pixel/mm. Therefore, each pixel represents 70 μm. With this in mind, each particle ($d_p = 1.8$ mm) was resolved at approximately 27 pixel per diameter. A detailed description of the technical and operational parameters is given in "Experimental setup" section.

Individual particles are recognized by correlating the sample image with image sections of the same size. Shifting the sample image pixel by pixel, the whole image is scanned and correlation coefficients are obtained. Correlation maxima are assigned to particle centroids, using a standard peak-finder. The threshold value for the correlation coefficient has been set to 0.6. This value ensures reasonable particle detection in terms of number of detected particles (872 particles in the exemplary image of Fig. 2) and quality. The latter means that particle overlap is almost completely excluded for a correlation coefficient of 0.6 or higher. The number of detected particles as a function of the threshold value is shown in Fig. 2. The chosen correlation coefficient is independent of the material properties. It can be applied to particles of different sizes, as long as the spatial resolution (27 pixel per diameter) is retained. This means larger particles can be captured in a larger field of view, whereas smaller particles require smaller fields of view. Consequently, the maximum number of particles in one image does not change. Increasing the total number of particles in a system increases the number of measurement locations required to capture all particles in the apparatus. All particle centers (x- and y-positions) are stored for further use in the tracking step.

Particle assignment using the Voronoi method

Particle tracking is carried out by identifying the same particle in two consecutive images. As this is a serious problem in dense particle systems, we use the Voronoi method proposed by Capart et al. (2002). They pointed out the advantages of the geometric, kinematic, and computational properties of Voronoi diagrams, and described the use of this information for particle assignment. The processing always runs with two consecutive images, which we call I_1 and I_2. The individual steps of the algorithm are now introduced, and the overall process is visualized in Fig. 3.

1. To generate Voronoi tessellations for both images based on previously detected particle centroids. The resulting polygons are stable in terms of shape and neighbors over several time steps,

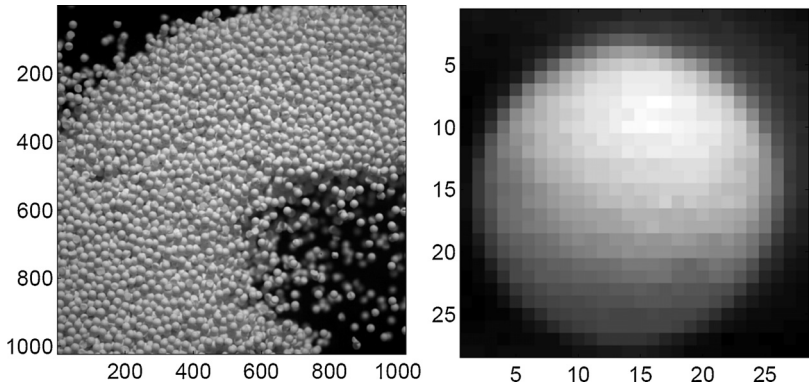

Fig. 1. An intensity corrected raw image (left) and the extracted sample particle image (right).

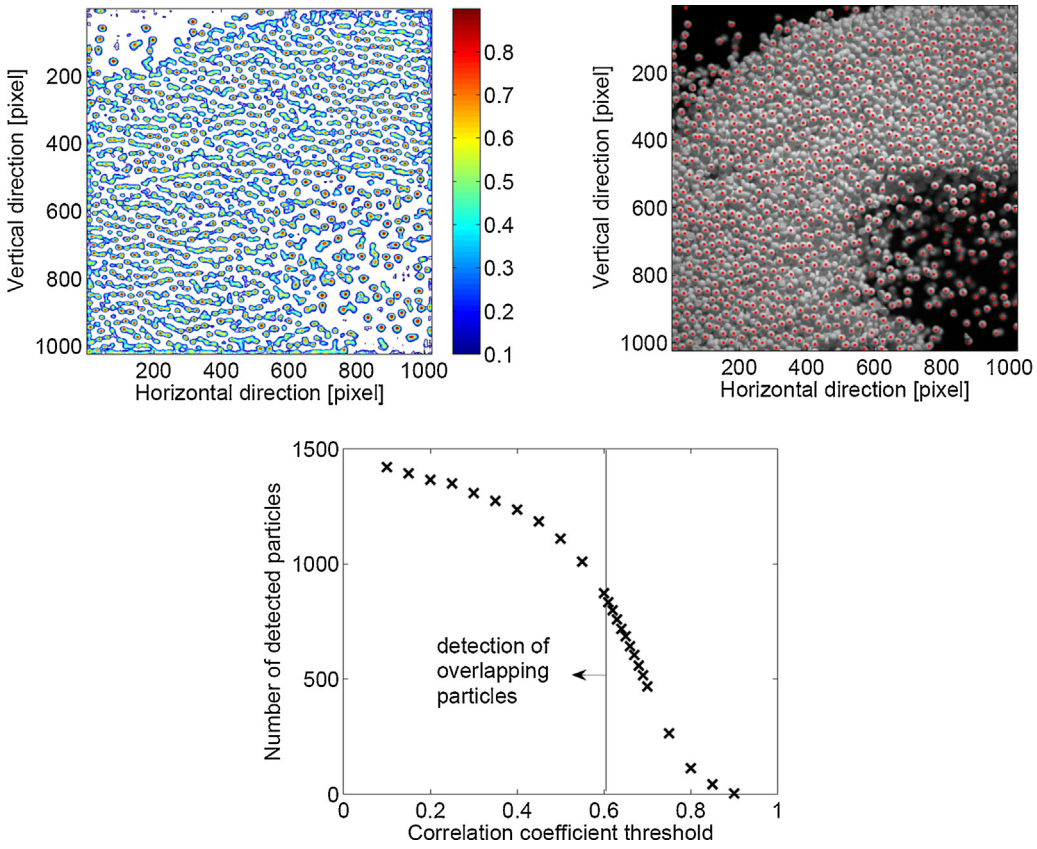

Fig. 2. Matrix of correlation coefficients (top, left), assigned particle centroids at a threshold value of 0.6 (top, right), number of detected particles as a function of threshold value (bottom).

as can be seen in Fig. 3. This step is carried out once for each pair of consecutive images. The following steps are repeated for each particle found in I_1.

2. For each centroid in I_1, the distance to all centroids in I_2 is calculated, and the three nearest neighbors are identified based on their distance. The Voronoi cell properties of these nearest neighbors are compared to identify the best match for each centroid of I_1 in I_2.
3. The most important feature of the Voronoi cells is represented by the Voronoi star S. Voronoi stars are made up of all connections between a centroid and its neighboring centroids, computed for the three nearest neighbors (called $S_{j,1-3}$), as well as for the centroid in I_1 (called $S_{i,1}$).
4. To evaluate the matching, the stars are translated so that their centroids coincide. Furthermore, irrespective of the number of branches in the individual stars, the minimum distance from each extremity of $S_{i,1}$ to the nearest extremities of $S_{j,1-3}$ are calculated and stored in a vector.
5. The median values of these vectors yield information about the quality of the matching. The minimal median corresponds to the best match and, when it does not exceed a threshold value, the median is used to assign the relevant particle in I_2 to each particle in I_1. The threshold value is set to $d_p/2.5$ pixel, which corresponds to a displacement of all neighboring particles of less than one particle radius. This value was found to almost completely exclude mismatches.
6. The displacement δ between two corresponding centroids in I_1 and I_2 is measured, and the particle velocity computed, by combining the displacement with the frame rate f_r used during the image acquisition process.

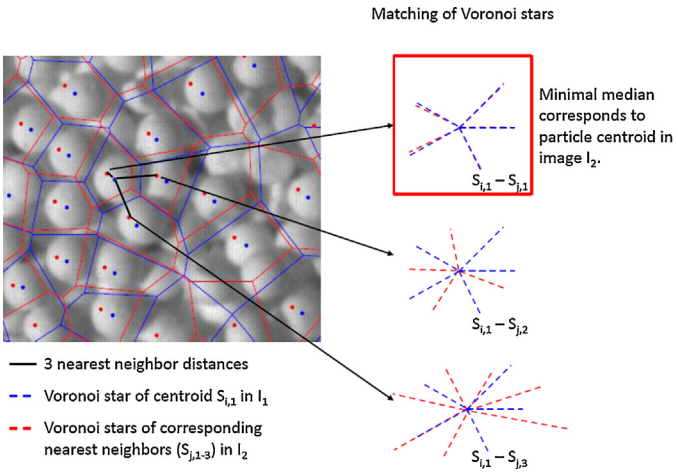

Fig. 3. Schematic of the steps in the Voronoi algorithm, including Voronoi tessellations for two time steps t_1 (blue) and $t_1 + \Delta t$ (red), search for nearest neighbors, calculation of Voronoi stars $S_{i,1}$ and $S_{j,1-3}$, and evaluation of Voronoi star matching by computing the median of extremity distances. (For interpretation of the references to color in figure legend, the reader is referred to the web version of the article.)

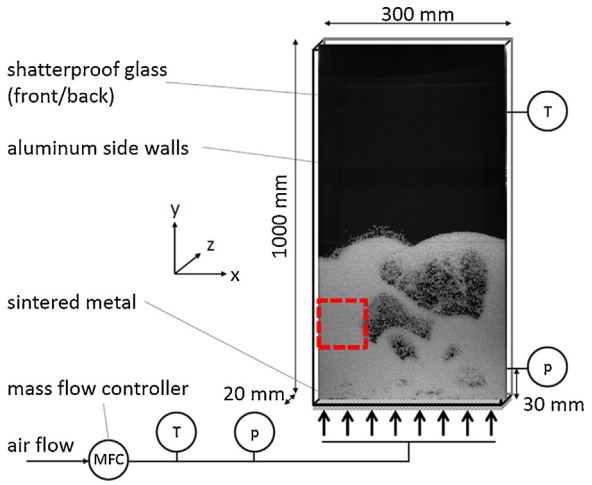

Fig. 4. Sketch of the pseudo-2D fluidized bed apparatus with dimensions, controls, and instruments; the field of view is represented by the red box. (For interpretation of the references to color in figure legend, the reader is referred to the web version of the article.)

Additional filter operations have been applied to exclude the double allocation of particles to the same particle in the next image I_2, and to avoid unrealistic particle velocities. The double allocation of particles might occur in the case of degeneration of Voronoi cells. If a particle in I_2 is assigned twice, the Voronoi stars are re-evaluated by repeating Steps 4 and 5 of the algorithm. The minimum median value determines which particle centroid in I_1 is assigned to the centroid in I_2, while the other one is deleted from the list of assignments. To prevent unrealistic particle velocities, we define the maximum allowable particle displacement as one particle radius per time step. This is reasonable based on the manual tracking of colored tracer particles, which never moved farther than this maximum value, even for fast particle motion within rising bubbles.

Experimental setup

Experiments were conducted using Geldart class D γ-alumina particles of diameter $d_p = 1.8$ mm and density $\rho_p = 1040$ kg/m^3. The solid (totaling 0.5 kg) was fluidized in the pseudo-2D bed illustrated in Fig. 4. We use the term "pseudo-2D" because the macroscopic appearance of the equipment suggests the 2D flow behavior of the particles. However, the detailed measurements show that particles move in all three dimensions, particularly in dilute particle-laden regions of gas bubbles and the freeboard. The process chamber measures 300 mm (width) × 1000 mm (height) × 20 mm (depth). The front and back are made of shatterproof glass, and the side walls are aluminum.

The planar PTV approach used in this study measured the vertical and horizontal velocity components of particles detected close to the transparent front wall. This boundary was covered with a thin plastic sheet to prevent abrasion. Friction effects were also reduced by the smooth surface of the plastic film. However, the particle velocities were assumed to decrease slightly when the particles were in direct contact with the front wall.

A sintered metal plate of 3 mm thickness served as the gas distributor, and a mass flow controller yielded the desired air flow rate. Tests for this feasibility study were conducted with an air flow rate of 20 kg/h, which corresponds to 1.4 times the minimum fluidization velocity ($u_{mf} = 0.56$ m/s).

The main component of our high-speed imaging system was a 1024 × 1024 pixel Photron high-speed camera with a CMOS chip. The camera was installed on a solid mounting frame in front of the process chamber, together with two 1100 W halogen lamps. It was operated at full resolution with a frame rate of 1000 fps, an exposure time of 1/31,000 s, and a dynamic range of 10 bits. To give the minimum depth of field and maximum light exposure, an objective lens with a 60 mm focal length and f-number of 4 was employed. The system was controlled using the DaVis image acquisition software (LaVision GmbH, Germany).

Images of size 71 mm × 71 mm were captured. Therefore, approximately one quarter of the chamber width was resolved with every image. The field of view (FOV) was localized in the upper third of the particle bed (approximately 120 mm above the bottom) and aligned with the left wall of the chamber. Two significant features of bubbling fluidized beds can be observed in this region, namely the upward transport of particles due to rising gas bubbles and particles sliding down the chamber wall.

Tests with lower resolutions and larger FOVs were conducted, but yielded worse particle segmentation behavior in terms of quantity and quality. An improved resolution with smaller FOV would result in even better particle segmentation. However, the rather small FOV does not reproduce the particle dynamics in a considerable part of the chamber, but yields only local particle information. Consequently, the image size serves as a compromise between required particle resolution and desired FOV for the current hardware.

Only a few images were required to assess whether PTV based on the Voronoi method could be applied to particles in bubbling fluidized beds. Finally, 200 images were captured and processed, corresponding to 0.2 s process time.

Results and discussion

The primary data delivered by PTV are the trajectories of individual particles as a Lagrangian representation of particle motion. An example of the particle tracks is shown in Fig. 5. The trajectories in the figure have been limited in length to 20 time steps ($\Delta t = 0.02$ s) to improve readability. The color coding represents the local and instantaneous magnitude of the particle velocity. An even better representation of the particle trajectories is given by

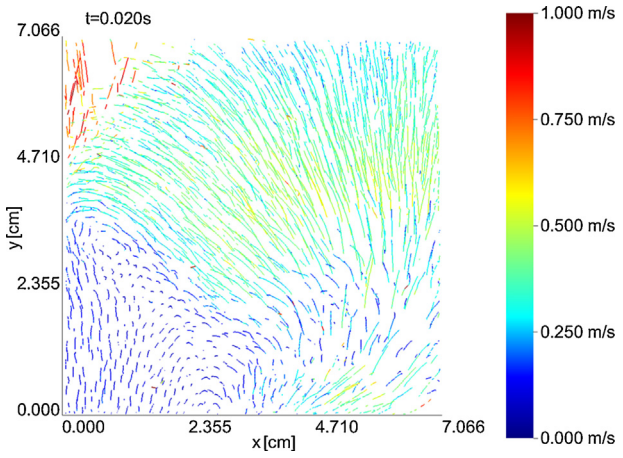

Fig. 5. Particle trajectories over the first 20 time steps, colored according to local/instantaneous particle velocity magnitude. (For interpretation of the references to color in figure legend, the reader is referred to the web version of the article.)

analyzing the time series, as shown in Appendix A (Fig. A1) and the video sequences in the supplementary material.

We also evaluated the length of individual trajectories. In Fig. 6, the distribution of the lifetime of individual trajectories shows how many trajectories have been observed. The total of 9585 trajectories corresponds to the absolute number of initiated trajectories, 872 of which were started directly with the first image-pair. Obviously, the lifetime of trajectories that commenced near to the end of the image sequence is limited by the length of the image sequence. The overall lifetimes (see right-hand side plot in Fig. 6) range from 1 ms (trajectory only visible on one image-pair) to 200 ms, which means that the particle was tracked over the complete image sequence. The average lifetime of all trajectories, indicated as a dotted line in Fig. 6, is $\tau = 13.23$ ms. A corrected lifetime of $\tau_{corr} = 15.97$ ms can be obtained by considering the limitation imposed by the limited length of the image sequence. Consequently, only the first 7000 trajectories have been evaluated—those that seem to be unaffected by the length of the sequence, based on a visual inspection of the lifetime cut-off. The cut-off is represented by the constant rate at which the trajectory lifetimes decrease to zero with increasing trajectory ID (identity number). Both the average and corrected lifetimes appear rather short compared to the total sequence time ($t_{total} = 200$ ms), but one must bear in mind that the total number of trajectories includes disconnected trajectories for the same particle. The reconstruction of trajectories is the main task for future work, and has not been considered up to now. Connecting the correct trajectories is a complex operation because of particle collisions and associated discontinuous movements.

Further meaningful information concerning the solid volume fraction, granular temperature, and Eulerian particle velocity field can be derived from the PTV results by averaging on the basis of interrogation areas. We applied an interrogation area of 128×128 pixel with a 75% overlap to compute the corresponding field data. The overlap was chosen to obtain a finer resolution of the field data.

Solid volume fraction

The solid volume fraction ε_p was obtained from the number of particles detected in each interrogation area. Based on the assumption that particles are segmented only if they exist in the first layer at the front glass wall, the detection volume can be defined as the product of the interrogation area I_A and the particle diameter d_p. Relating the total volume of n segmented particles to the detection volume yields the local solid volume fraction

$$\varepsilon_p = \frac{(\pi/6)\sum_n d_{p,n}^3}{I_A d_p}. \quad (2)$$

The solid volume fraction at the instant that the previous particle trajectories started is shown in Fig. 7. The complete time series can be found in Appendix A (see Fig. A2). The particle distributions agree fairly well with the estimated volume fraction magnitudes. This method relies solely on discrete particle detection, and no additional calibration of light intensity is necessary. Therefore, the approach is advantageous compared to other optical methods used for volume fraction measurements, such as the digital image analysis described by Van Buijtenen et al. (2011). Nevertheless, minor errors occur because particles are detected even if they are blurred, or are not detected if they are visible only in fractions, i.e., along the edges. The volume fraction estimation is then less accurate, and an overall correction on the basis of the total bed mass is not possible, as we are capturing only a portion of the particles. Nonetheless, reasonable maximum values for the solid volume fraction ($\varepsilon_p \cong 0.6$ for a randomly packed static bed of mono-sized spheres) can be obtained, together with good qualitative agreement between the computed ε_p and the particle appearances in the raw images.

Granular temperature

Following Gidaspow (1994), the collision frequency of particles in granular flows can be described on the basis of the kinetic theory of granular flow. Analogous to the kinetic theory of gases, where the collision frequency is proportional to the gas temperature, the kinetic theory of granular flow associates the random velocity fluctuations of the particles to a "temperature" value, the so-called granular temperature. Consequently, the granular temperature is a measure for the particle collision rate. Specifically, the granular temperature T_{gran} can be derived from the fluctuations in the particle velocity (velocity variance σ_x^2 and σ_y^2 in the corresponding directions). If more than one particle is found in the interrogation area, the local velocity variance can be computed, and the granular temperature is given by

$$T_{gran} = \frac{1}{2}(\sigma_x^2 + \sigma_y^2). \quad (3)$$

To capture the large range of granular temperatures, Fig. 8 shows the logarithm of the instantaneous granular temperature. White spots denote regions with one or no particles detected, corresponding to a velocity variance of zero. Similar to the previous results, the complete time series is shown in Appendix A (Fig. A3).

Particle collisions are not estimated quantitatively. Nevertheless, regions with high granular temperatures are often associated with high particle collision rates. This phenomenon was observed in our experiments. Increased collision rates can often be observed along the boundary of larger particle assemblies. For instance, the particles sliding down the left wall are separated from the freeboard by a region of increased granular temperature. The same can be observed in later time steps, when a new bubble enters the FOV and transports particles upwards. At the same time, particles that are falling down collide with the rising particles (see lower-right corner of the images in Fig. A3). Thus, the granular temperature appears to be a measure of the collision frequency in larger-scale particle motion.

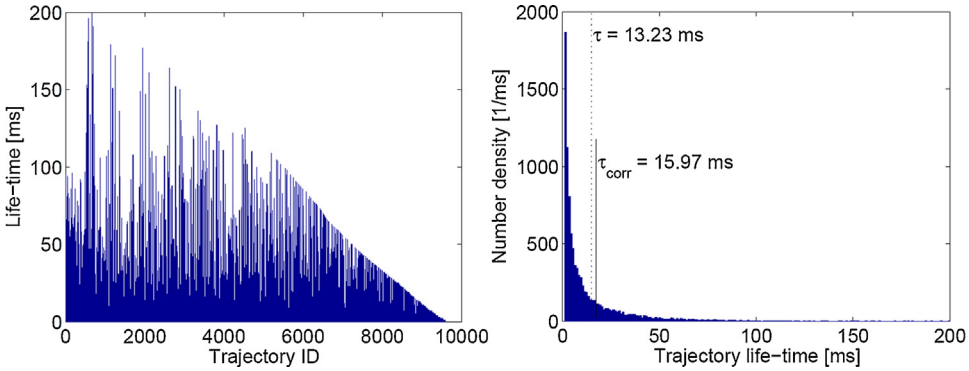

Fig. 6. Lifetime distribution of individual trajectories (left) and overall lifetime distribution (right).

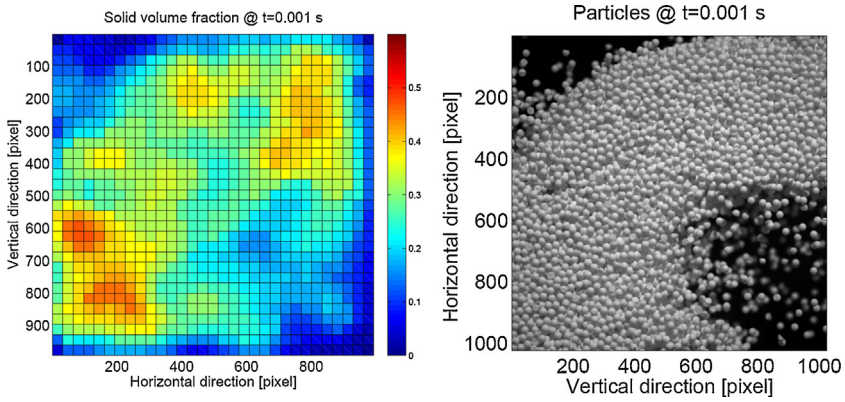

Fig. 7. Plot of instantaneous solid volume fraction ε_p together with particle distribution.

Eulerian description of particle motion

Moreover, the Eulerian description of particle motion can be approximated by averaging the individual particle velocity components. Following Miozzi and Querzoli (1996), a representative velocity vector can be derived for each interrogation area. The corresponding velocity field in the first time step is shown in the left-hand side image of Fig. 9 (complete time series shown in Fig. A4). Additionally, the Eulerian velocity field obtained from individual particle tracks has been compared with the results of standard PIV processing (Fig. 9, right-hand side image). The agreement between the images in Fig. 9 is reasonably good, with only minor deviations in velocity magnitude and the location of flow structures, for instance the vortex center (middle-left). Nevertheless, a good approximation of the solid phase velocity field is provided by averaging the PTV data. From this rough evaluation and comparison, it can be concluded that the PTV approach yields both a Lagrangian and Eulerian description of the particle dynamics.

More sophisticated analysis of the two flow fields is possible, e.g., using proper orthogonal decomposition, which is a common approach for complex, unsteady flows (Arányi, Janiga, Zähringer, & Thévenin, 2013). In future work, we will use proper orthogonal decomposition to assess the proposed PTV approach in comparison with the established PIV method.

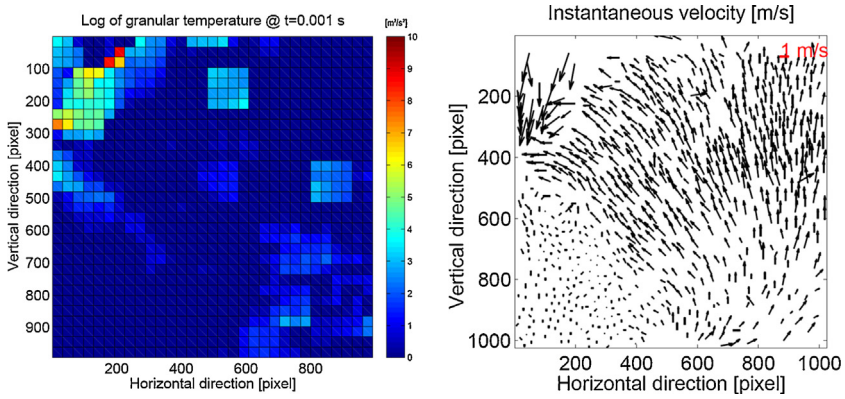

Fig. 8. Logarithmic plot of instantaneous granular temperature T_{gran} together with particle velocity vectors, with 1 m/s reference vector given in red in the upper right corner.

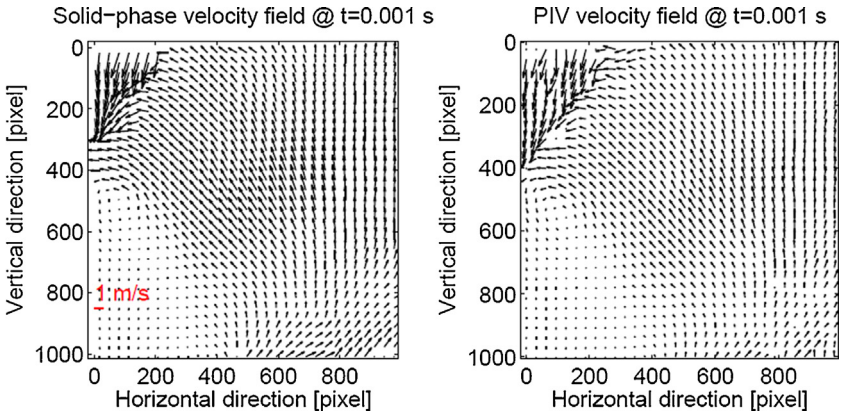

Fig. 9. Instantaneous solid phase velocity field obtained by averaging individual particle velocities from PTV (left) and solid phase velocity field obtained by standard PIV algorithm (right).

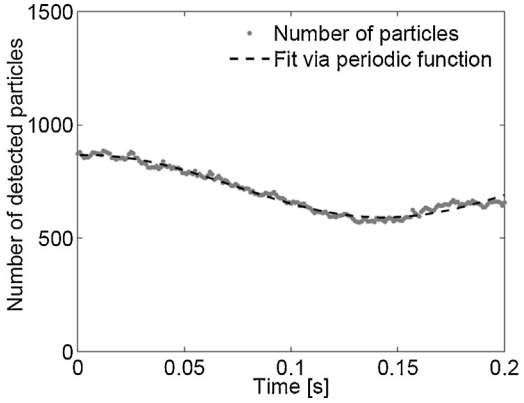

Fig. 10. Temporal evolution of the number of detected particles in the FOV.

Furthermore, we will consider the influence of the FOV on the results that can be obtained. At present, the results appear to be significant and representative of the whole particle system. This can be concluded from just 200 images, based on the temporal evolution of the number of detected particles. As shown in Fig. 10, the curve progresses steadily over more than half the period of a frequency of approximately 3 Hz. This corresponds to the typical bubble formation frequency at a fluidization velocity of $1.4\,u_{mf}$ for Geldart class D particles (He et al., 2014).

Conclusions

We have reported the application of a combined PTV and Voronoi method to the motion of particles in a fluidized bed. Contrary to previous applications in Couette shear cells, hoppers, and vibrating beds, this is the first time that large numbers of individual particles have been tracked under the fluctuating flow conditions of a bubbling fluidized bed.

Coupling high-speed imaging with an innovative segmentation approach and the Voronoi algorithm, we acquired particle velocities in densely packed bed regions as well as in dilute regions of rising bubbles. The varied particle dynamics that are usually found in rising bubbles or dense particle beds can be captured, regardless of the direction of particle motion or velocity magnitude.

Applying a local averaging procedure over interrogation areas, further evaluation of the Lagrangian information (particle trajectories) yielded instantaneous granular temperature fields and the spatial distribution of the solid volume fraction. The latter assumes that the observation is restricted to a depth of field of one particle diameter. The limited quality of this simplified approach could be overcome in future work by using stereoscopic imaging, as described by Spinewine, Capart, and Zech (2002).

The solid-phase velocity fields (Eulerian description) can also be obtained. We observed good agreement between the approximated velocity field and that obtained by a standard PIV approach, with only minor deviations in velocity magnitudes and flow field structures. However, such deviations seem to be insignificant, suggesting the proposed PTV method is comparable to the established technique of PIV.

The possibility to detect particle collisions makes the proposed approach particularly attractive. Although this paper has only evaluated particle collisions in a qualitative manner, further research should provide quantitative information on the particle-particle and particle-wall collision frequencies.

Technical hardware developments will improve our ability to observe larger areas with more and smaller particles. This is expected to greatly enhance the validation and improvement of macroscopic models for particle formulation processes.

Acknowledgement

The authors gratefully acknowledge the funding of this work by the German Federal Ministry of Science and Education (BMBF) as part of the InnoProfile-Transfer project NaWiTec (03IPT701X). We also thank Christian Knopf for supporting the experiments in the framework of his MSc thesis.

Appendix A. Time series data

The temporal evolution of particle positions and the visualization of corresponding quantities confirm the potential of the PTV technique to analyze granular flows. In particular, the time series of the estimated quantities (shown in this section and video sequences available online) can be used to conduct a detailed analysis of the particle dynamics. The results are highly resolved in time and space, and are therefore an appropriate source for the sophisticated validation of numerical simulations such as coupled CFD-DEM simulations. This appendix presents the time series results for particle trajectories in Fig. A1, solid volume fraction in Fig. A2, granular temperature in Fig. A3, and Eulerian solid-phase flow field in Fig. A4.

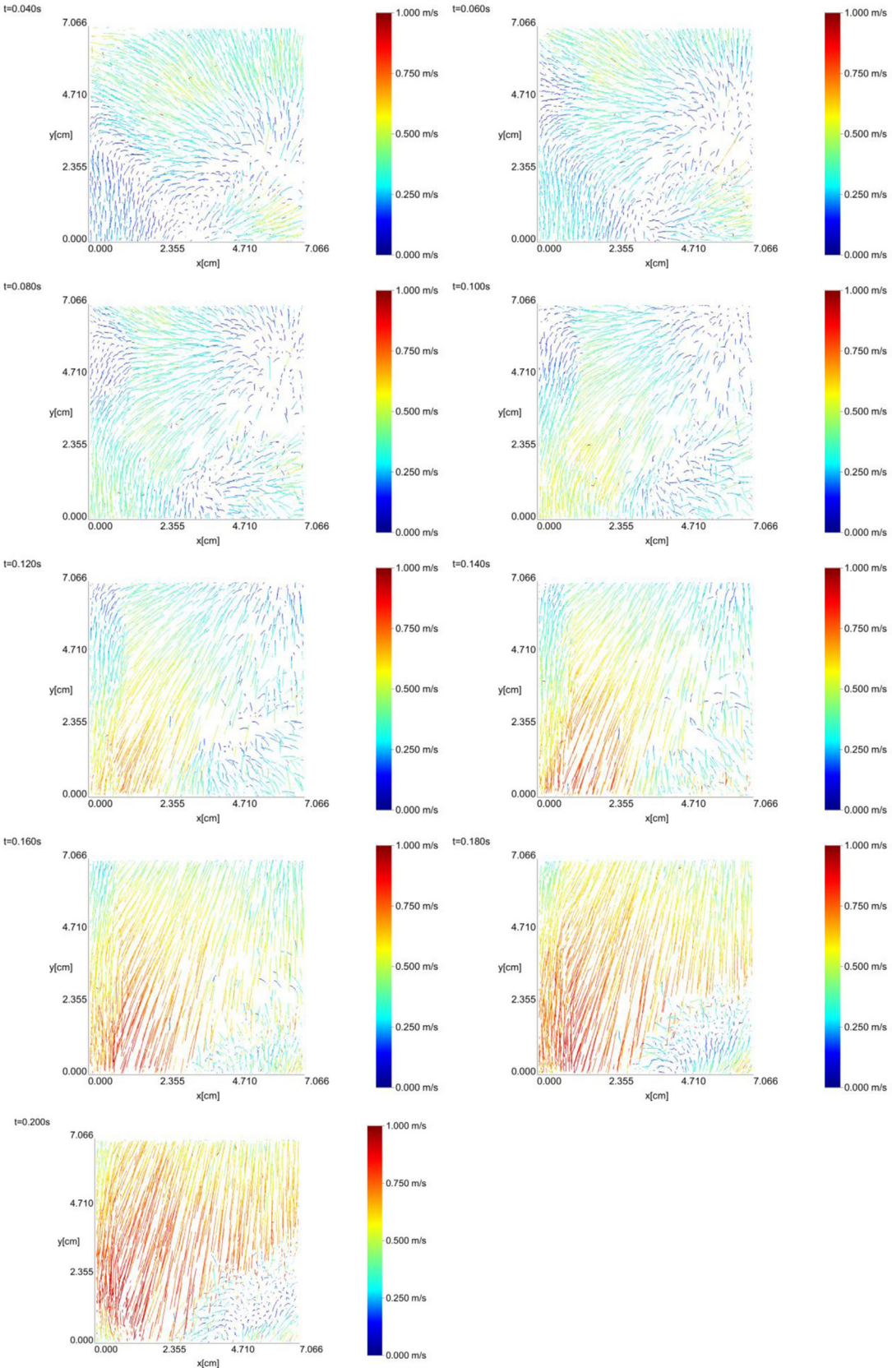

Fig. A1. Particle trajectories over 20 time steps, colored in terms of local/instantaneous particle velocity magnitude, as time series starting from the top-left corner going to the lower-right corner with time steps of $\Delta t = 20$ ms.

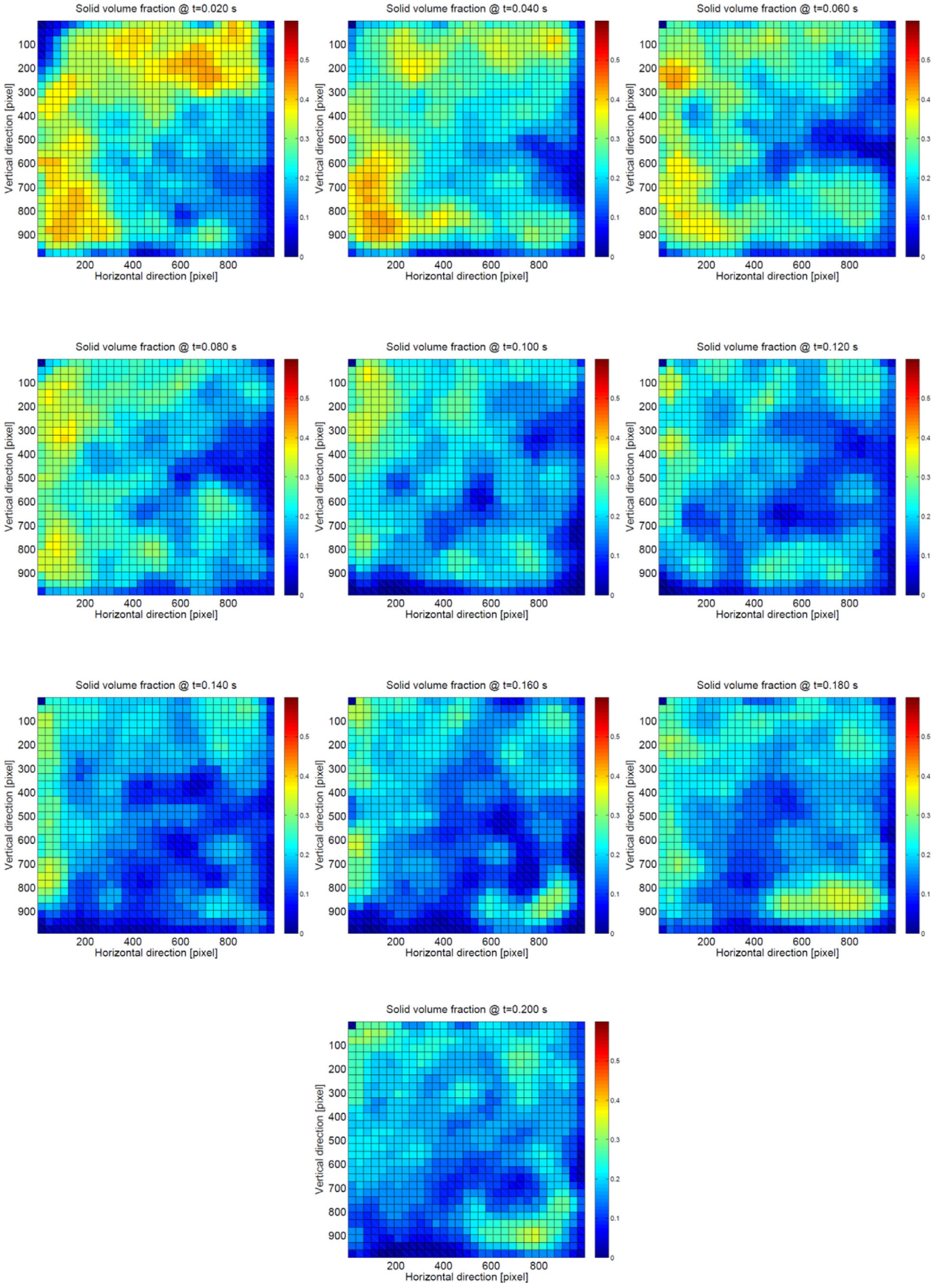

Fig. A2. False color plots of instantaneous solid volume fraction ε_p as time series with $\Delta t = 20$ ms.

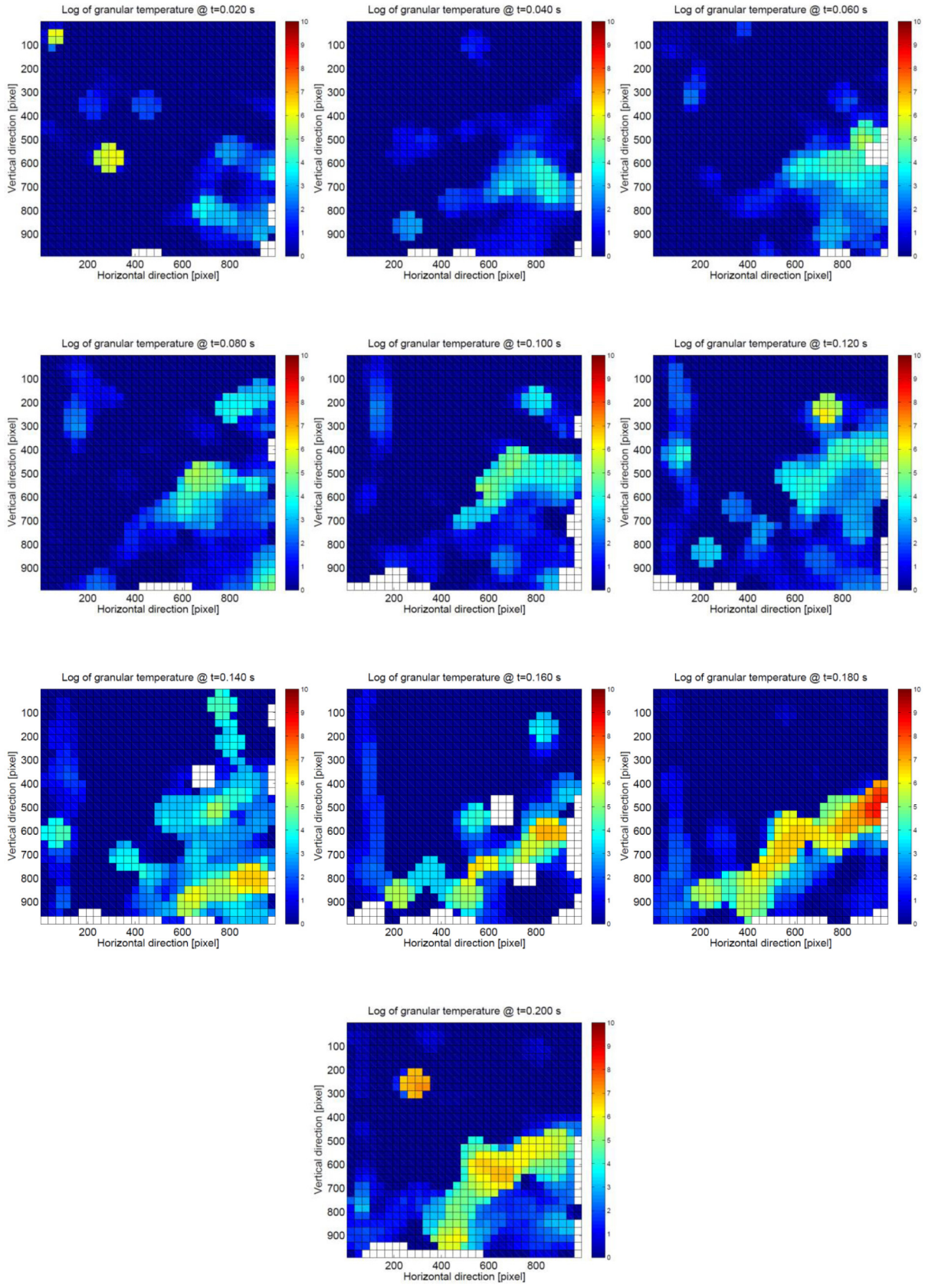

Fig. A3. False color plots of the logarithm of instantaneous granular temperature T_{gran} as time series with $\Delta t = 20$ ms.

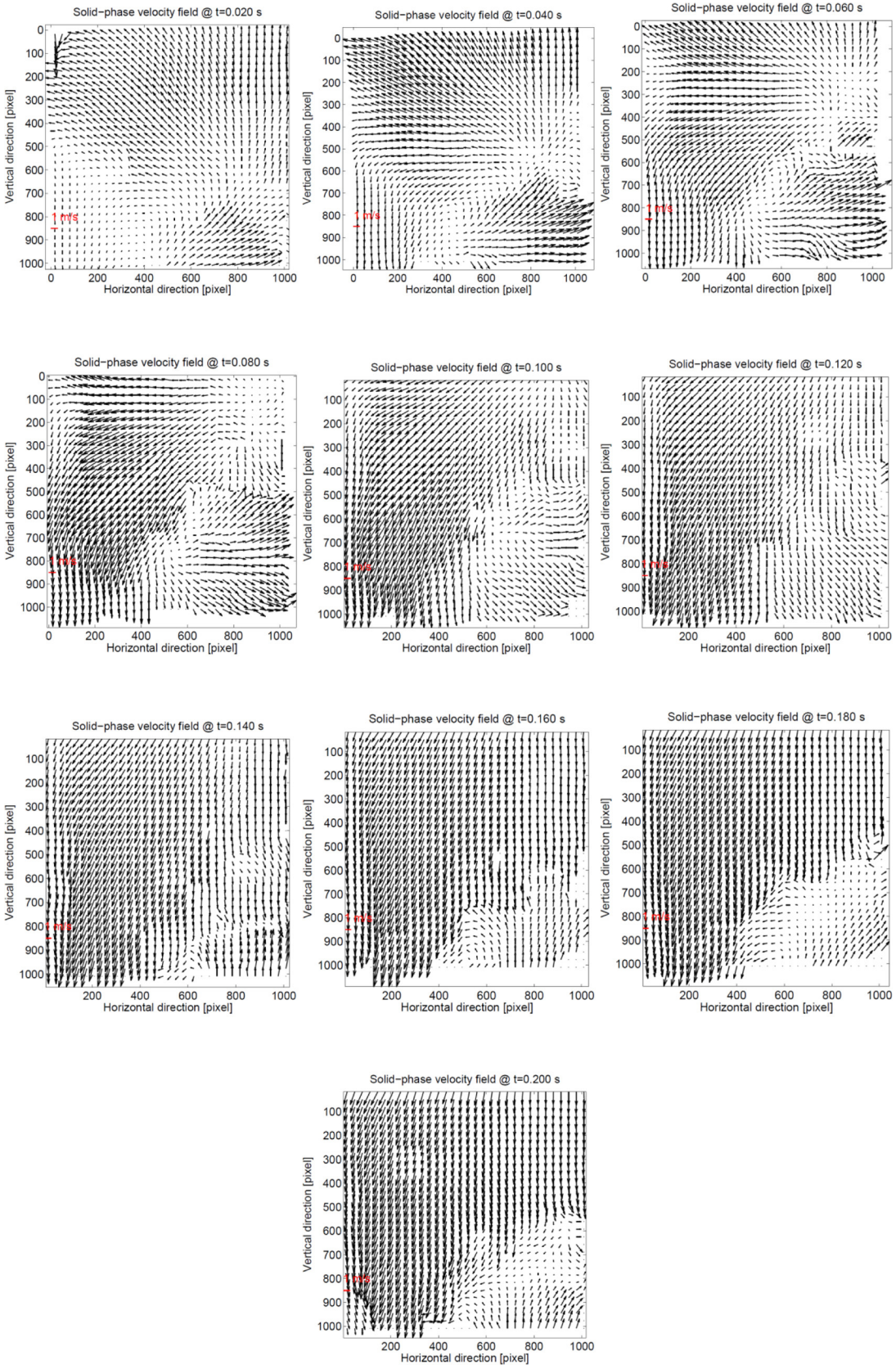

Fig. A4. Approximated, instantaneous solid-phase velocity fields as time series with $\Delta t = 20$ ms, with 1 m/s reference vector given in red in the lower-left corner.

Appendix B. Supplementary data

Supplementary data associated with this article can be found, in the online version, at http://dx.doi.org/10.1016/j.partic.2014.08.004.

References

Adrian, R. (1991). Particle-imaging techniques for experimental fluid mechanics. *Annual Review of Fluid Mechanics*, *23*, 261–304.

Aleixo, R., Soares-Frazão, S., & Zech, Y. (2011). Velocity-field measurements in a dam-break flow using a PTV Voronoi imaging technique. *Experiments in Fluids*, *50*, 1633–1649.

Arányi, P., Janiga, G., Zähringer, K., & Thévenin, D. (2013). Analysis of different POD methods for PIV-measurements in complex unsteady flows. *International Journal of Heat and Fluid Flow*, *43*, 204–211.

Aurenhammer, F. (1991). Voronoi diagrams—A survey of a fundamental geometric data structure. *ACM Computing Surveys (CSUR)*, *23*, 345–405.

Bendicks, C., Tarlet, D., Roloff, C., Bordás, R., Wunderlich, B., Michaelis, B., et al. (2011). Improved 3-D particle tracking velocimetry with colored particles. *Journal of Signal and Information Processing*, *2*(2), 59–71.

Bhusarapu, S., Al-Dahhan, M., & Duduković, M. (2006). Solids flow mapping in a gas-solid riser: Mean holdup and velocity fields. *Powder Technology*, *163*, 98–123.

Börner, M., Hagemeier, T., Ganzer, G., Peglow, M., & Tsotsas, E. (2014). Experimental spray zone characterization in top-spray fluidized bed granulation. *Chemical Engineering Science*, *116*, 317–330.

Börner, M., Peglow, M., & Tsotsas, E. (2013). Derivation of parameters for a two compartment population balance model of Wurster fluidised bed granulation. *Powder Technology*, *238*, 122–131.

Capart, H., Young, D. L., & Zech, Y. (2002). Voronoi imaging methods for the measurement of granular flows. *Experiments in Fluids*, *32*, 121–135.

Chou, H. T., & Lee, C. F. (2009). Cross-sectional and axial flow characteristics of dry granular material in rotating drums. *Granular Matter*, *11*, 13–32.

Chung, Y., Hsiau, S., Liao, H., & Ooi, J. (2010). An improved PTV technique to evaluate the velocity field of non-spherical particles. *Powder Technology*, *202*, 151–161.

Crowe, C. (2006). *Multiphase flow handbook*. Boca Raton: Taylor & Francis Group.

Crowe, C., Sommerfeld, M., & Tsuji, Y. (1998). *Multiphase flows with droplets and particles*. New York: CRC Press.

Fries, L., Antonyuk, S., Heinrich, S., & Palzer, S. (2011). DEM – CFD modeling of a fluidized bed spray granulator. *Chemical Engineering Science*, *66*, 2340–2355.

Gidaspow, D. (1994). *Multiphase flow and fluidization: Continuum and kinetic theory descriptions*. New York: Academic Press.

He, H., Lu, X., Shuang, W., Wang, Q., Kang, Y., Yan, L., et al. (2014). Statistical and frequency analysis of the pressure fluctuation in a fluidized bed of non-spherical particles. *Particuology*, *16*, 178–186.

Hsiau, S. S., & Jang, H. W. (1998). Measurements of velocity fluctuations of granular materials in a shear cell. *Experimental Thermal and Fluid Science*, *17*, 202–209.

Jesuthasan, N., Baliga, B., & Savage, S. (2006). Use of particle tracking velocimetry for measurements of granular flows: Review and application-particle tracking velocimetry for granular flow measurements. *KONA Powder and Particle Journal*, *24*, 15–26.

Lloyd, P., Ball, D., & Standsby, P. (1995). Unsteady surface-velocity field measurement using particle tracking velocimetry. *Journal of Hydraulic Research*, *33*, 519–534.

Luchnikov, V., Medvedev, N., Oger, L., & Troadec, J. P. (1999). Voronoi–Delaunay analysis of voids in systems of nonspherical particles. *Physical Review E*, *59*, 7205–7212.

Lun, C., Savage, S., Jeffrey, D., & Chepurniy, N. (1984). Kinetic theories for granular flow: Inelastic particles in Couette flow and slightly inelastic particles in a general flow field. *Journal of Fluid Mechanics*, *140*, 223–256.

Miozzi, M., & Querzoli, G. (1996). PTV and POD analysis of the instabilities in a quasi two-dimensional convective flow. *Applied Scientific Research*, *56*, 221–242.

Natarajan, V., Hunt, M., & Taylor, E. (1995). Local measurements of velocity fluctuations and diffusion coefficients for a granular material flow. *Journal of Fluid Mechanics*, *304*, 1–25.

Sommerfeld, M. (2001). Validation of a stochastic Lagrangian modeling approach for inter-particle collisions in homogeneous isotropic turbulence. *International Journal of Multiphase Flow*, *27*, 1829–1858.

Spinewine, B., Capart, H., Larcher, M., & Zech, Y. (2003). Three-dimensional Voronoi imaging methods for the measurement of near-wall particulate flows. *Experiments in Fluids*, *34*, 227–241.

Spinewine, B., Capart, H., & Zech, Y. (2002). Three-dimensional Voronoi imaging methods for the simultaneous measurement of velocities and concentrations in dense particulate flows. In *Proceedings of Hydraulic Measurements and Experimental Methods* Estes Park, USA, (pp. 1–10).

Spinewine, B., & Zech, Y. (2001). Digital imaging characterisation of a granular hopper flow. In *Proceedings of Partec—International Congress for Particle Technology* Nuremberg, Germany, (pp. 1–8).

Van Buijtenen, M., Börner, M., Deen, N., Heinrich, S., Antonyuk, S., & Kuipers, J. (2011). An experimental study of the effect of collision properties on spout fluidized bed dynamics. *Powder Technology*, *206*, 139–148.

Werther, J. (1999). Measurement techniques in fluidized beds. *Powder Technology*, *102*, 15–36.